



Microstructure evolution in wire-arc additively manufactured martensitic stainless steel

Jules L'HOSTIS, Marie-Noëlle AVETTAND-FÈNOËL and Ludovic THUINET

Univ. Lille, CNRS, INRAE, Centrale Lille, UMR 8207 - UMET - Unité Matériaux et Transformations,
F-59000 Lille, France

Table of contents

Introduction

Materials and process parameters

Experimental results

 Hardness profile

 Nature, dimensions and localization of phases

Discussion

Conclusions & perspectives

Advantages of WAAM and martensitic stainless steels

Wire-arc additive manufacturing

- High deposition rate.
 - Large parts
 - Already available welding wires.
 - No use of dangerous powders.
 - Ability to repair already built parts.
- ✗ Low spatial resolution.
- ✗ Bad surface finish.

Martensitic SS steel : ER410 NiMo

- Applications for water and steam turbines.
- Lack of literature on additive manufacturing of martensitic stainless steels.
- Complex solid-state transformations.

How is the solidified microstructure affected by thermal cycles caused by subsequent layers deposition ?

Chemical composition of filler wire & substrate

Table: ER410 NiMo filler wire and 304L substrate chemical composition (mass. %).

mass. %	Fe	C	Cr	Ni	Mo	Si	Mn	N	O	P	Cu
ER410 NiMo	81.3	0.025	12.6	4.7	0.44	0.4	0.38	0.022	0.005	0.018	0.051
304L	70.8	0.028	17.9	8.1	0.45	0.33	1.88	0.002		0.041	0.376

Predicted phase transformation temperatures using ThermoCalc software and TCFE11 database :

$$Ac_3 = 730 \text{ } ^\circ\text{C} \quad Ac_1 = 580 \text{ } ^\circ\text{C} \quad M_s = 270 \text{ } ^\circ\text{C} \quad M_f = 120 \text{ } ^\circ\text{C}$$

WAAM building parameters

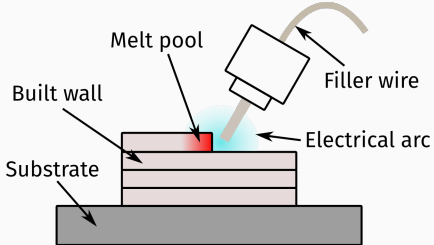


Figure: WAAM principle.

- 30 layers.
- Thin wall : single bead layers.
- Unidirectional deposition path.
- Temperature measurements with K-type thermocouples.

Table: Deposition parameters.

CMT voltage	14.8 V
CMT current	109 A
CMT arc regime	dynamic 3551
Scanning speed	50 cm/min
Feeding speed	4 m/min
Wire diameter	1.2 mm
Stick out distance	15 mm
Gas flow rate (Ar + 2%CO ₂)	16 L/min
Deposition rate	2.13 kg/h
Deposition energy	2.6 kJ/cm

Built wall dimensions and features

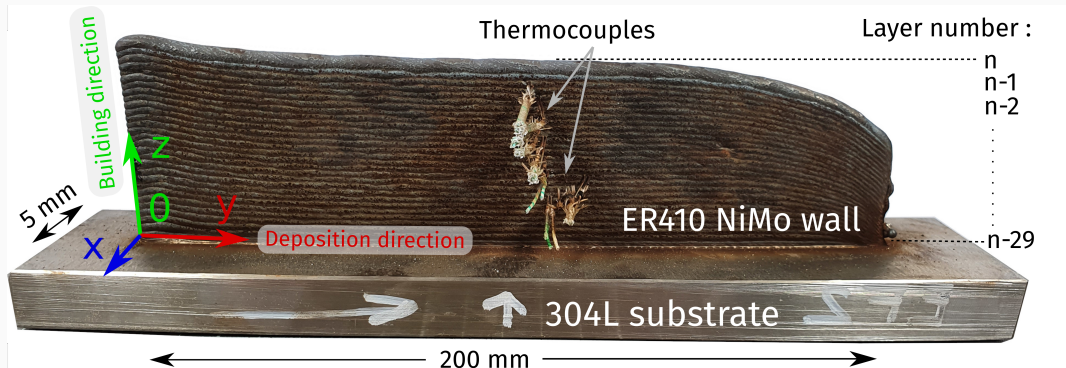


Figure: WAAM built thin wall, made at Institut de soudure de Yutz. 200 mm long, 5 mm wide, 30 layers tall.

A sound ER410 NiMo thin wall was successfully built using WAAM and thermocouples were stuck in different layers to record thermal cycles.

The following micrographs are taken from (\vec{x}, \vec{z}) transversal sections of the wall.

Measured thermal cycles

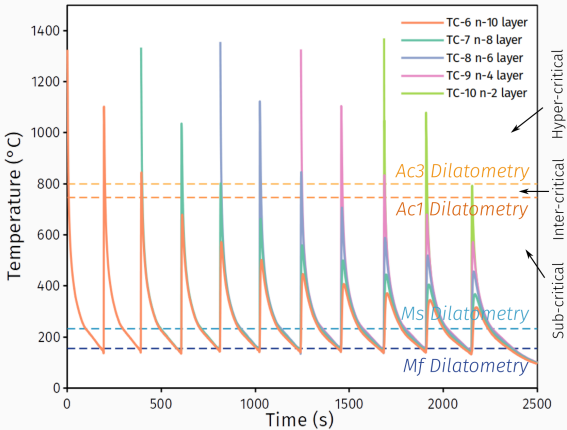


Figure: Measured thermal cycles in every 2 layers in the last 11 ones.

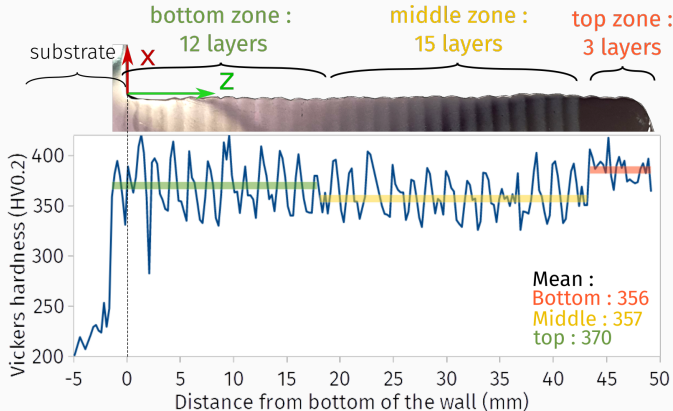
Table: Comparison of phase transformation temperatures.

Temp. (°C)	Ac ₃	Ac ₁	M _s	M _f
ThermoCalc	730	580	270	120
Dilatometry	800	747	232	156

Interpass temperature :
 $T_{interpass} = 150 \text{ }^{\circ}\text{C} \approx M_f$.

- First 2 reheatings : $T_{peak} > Ac_3$.
- 3rd and more : $T_{peak} < Ac_1$

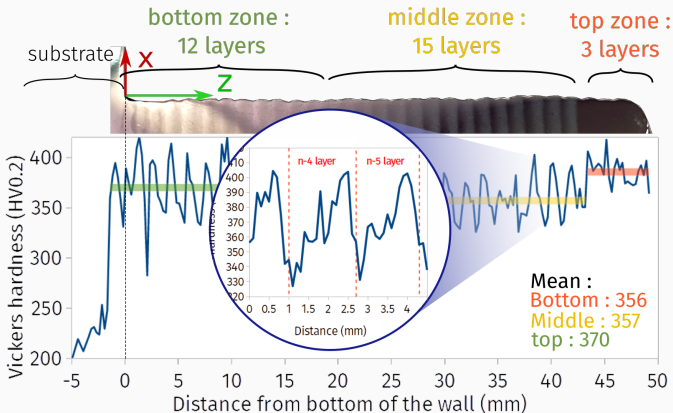
Several zones along building direction



- 3 zones depending on thermal conditions.

Figure: Hardness evolution along the building direction.
Transversal section of the wall etched with Villela's reagent for
30 s.

Several zones along building direction



- 3 zones depending on thermal conditions.
- Hardness oscillation in each layer (except for top zone).

Figure: Hardness evolution along the building direction.
Transversal section of the wall etched with Villela's reagent for
30 s.

Several zones along building direction

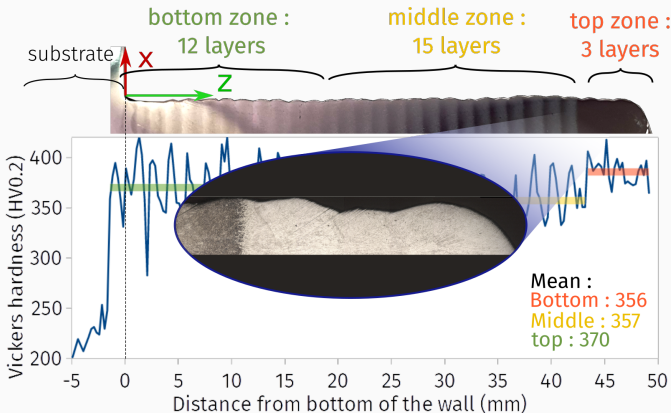
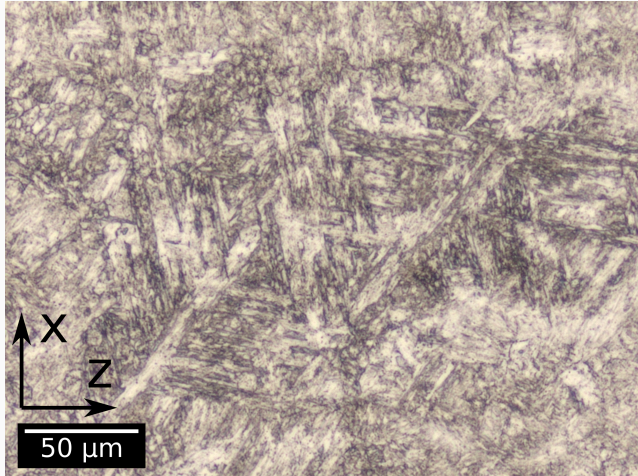


Figure: Hardness evolution along the building direction.
Transversal section of the wall etched with Villela's reagent for
30 s.

- 3 zones depending on thermal conditions.
- Hardness oscillation in each layer (except for top zone).
- Different etching response in top zone.

Top zone composed of the 3 lastly built layers.
These layers were fully austenitized by the last reheating.

The martensitic microstructure



- Low carbon content (0.025 mass.%): lath-shaped martensite.

Figure: Optical micrograph of middle zone. Transversal section, Villela etching for 1 min.

Martensite architecture and prior austenite grain reconstruction

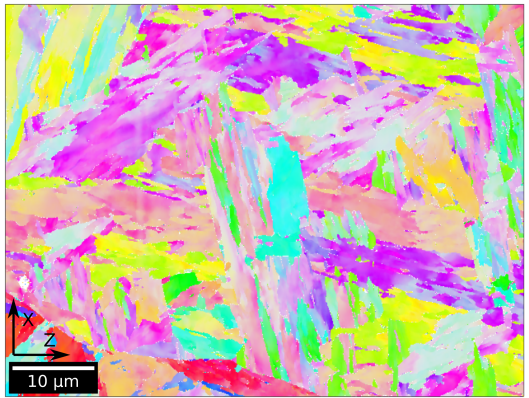


Figure: Inverse pole figure (Z) of n (lastly built) layer.

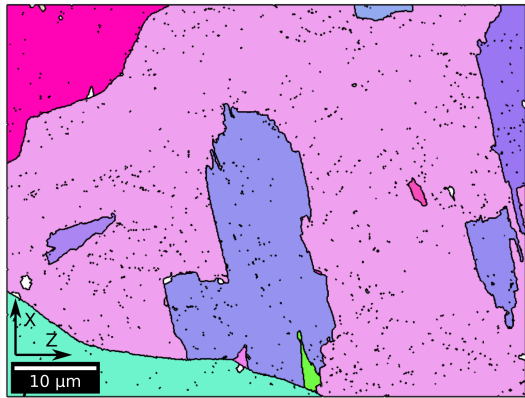
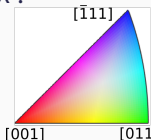


Figure: Reconstruction of prior austenite grain orientations with MTEX¹.

¹R. Hielscher et al., *Materialia* 2022, 22, 101399



Orientation relationship determination between γ and α'

O.R. ^a	fcc plane ^b	bcc plane	fcc direction ^c	bcc direction	Bain Variant ^d
KS1	(111) $_{\gamma}$	(011) $_{\alpha'}$	[101] $_{\gamma}$	[111] $_{\alpha'}$	B_3
KS2	(111) $_{\gamma}$	(011) $_{\alpha'}$	[101] $_{\gamma}$	[111] $_{\alpha'}$	B_1
KS3	(111) $_{\gamma}$	(011) $_{\alpha'}$	[110] $_{\gamma}$	[111] $_{\alpha'}$	B_1
KS4	(111) $_{\gamma}$	(011) $_{\alpha'}$	[110] $_{\gamma}$	[111] $_{\alpha'}$	B_2
KS5	(111) $_{\gamma}$	(011) $_{\alpha'}$	[011] $_{\gamma}$	[111] $_{\alpha'}$	B_2
KS6	(111) $_{\gamma}$	(011) $_{\alpha'}$	[011] $_{\gamma}$	[111] $_{\alpha'}$	B_3
KS7	(111) $_{\gamma}$	(011) $_{\alpha'}$	[101] $_{\gamma}$	[111] $_{\alpha'}$	B_1
KS8	(111) $_{\gamma}$	(011) $_{\alpha'}$	[101] $_{\gamma}$	[111] $_{\alpha'}$	B_3
KS9	(111) $_{\gamma}$	(011) $_{\alpha'}$	[110] $_{\gamma}$	[111] $_{\alpha'}$	B_2
KS10	(111) $_{\gamma}$	(011) $_{\alpha'}$	[110] $_{\gamma}$	[111] $_{\alpha'}$	B_1
KS11	(111) $_{\gamma}$	(011) $_{\alpha'}$	[011] $_{\gamma}$	[111] $_{\alpha'}$	B_3
KS12	(111) $_{\gamma}$	(011) $_{\alpha'}$	[011] $_{\gamma}$	[111] $_{\alpha'}$	B_2
KS13	(111) $_{\gamma}$	(011) $_{\alpha'}$	[101] $_{\gamma}$	[111] $_{\alpha'}$	B_1
KS14	(111) $_{\gamma}$	(011) $_{\alpha'}$	[101] $_{\gamma}$	[111] $_{\alpha'}$	B_3
KS15	(111) $_{\gamma}$	(011) $_{\alpha'}$	[110] $_{\gamma}$	[111] $_{\alpha'}$	B_2
KS16	(111) $_{\gamma}$	(011) $_{\alpha'}$	[110] $_{\gamma}$	[111] $_{\alpha'}$	B_1
KS17	(111) $_{\gamma}$	(011) $_{\alpha'}$	[011] $_{\gamma}$	[111] $_{\alpha'}$	B_3
KS18	(111) $_{\gamma}$	(011) $_{\alpha'}$	[011] $_{\gamma}$	[111] $_{\alpha'}$	B_2
KS19	(111) $_{\gamma}$	(011) $_{\alpha'}$	[101] $_{\gamma}$	[111] $_{\alpha'}$	B_1
KS20	(111) $_{\gamma}$	(011) $_{\alpha'}$	[101] $_{\gamma}$	[111] $_{\alpha'}$	B_3
KS21	(111) $_{\gamma}$	(011) $_{\alpha'}$	[110] $_{\gamma}$	[111] $_{\alpha'}$	B_2
KS22	(111) $_{\gamma}$	(011) $_{\alpha'}$	[110] $_{\gamma}$	[111] $_{\alpha'}$	B_1
KS23	(111) $_{\gamma}$	(011) $_{\alpha'}$	[011] $_{\gamma}$	[111] $_{\alpha'}$	B_3
KS24	(111) $_{\gamma}$	(011) $_{\alpha'}$	[011] $_{\gamma}$	[111] $_{\alpha'}$	B_2

^a KS j

^b $\mathbf{n}_j = (-1)^{j+1} P_j (111)_{\gamma}$

^c $P_j [101]_{\gamma}$

^d $B_j = P_j B_3 P_j^T$

Table: KURDJUMOV-SACHS variants list².

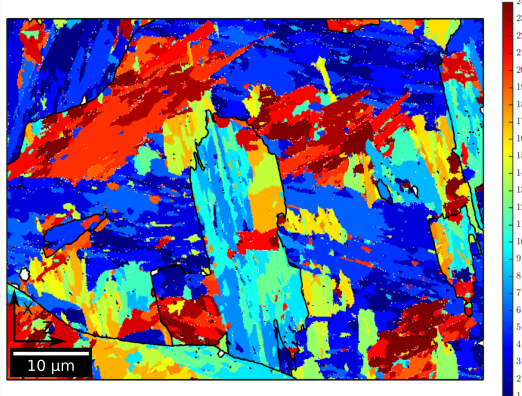


Figure: Variants indexation map.

Fit of OR model with experimental data

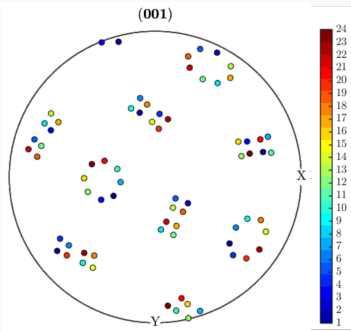


Figure: Rotated KS orientation relationships.

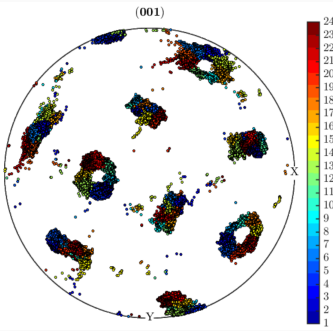


Figure: Pole figure of experimental variants orientations in 1 grain.

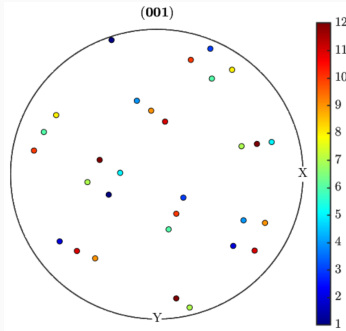


Figure: Rotated NW orientation relationships.

The experimental ORs lie between KURDJUMOV-SACHS and NISHIYAMA-WASSERMANN ORs, but are closer to KS.

Nature of the phases

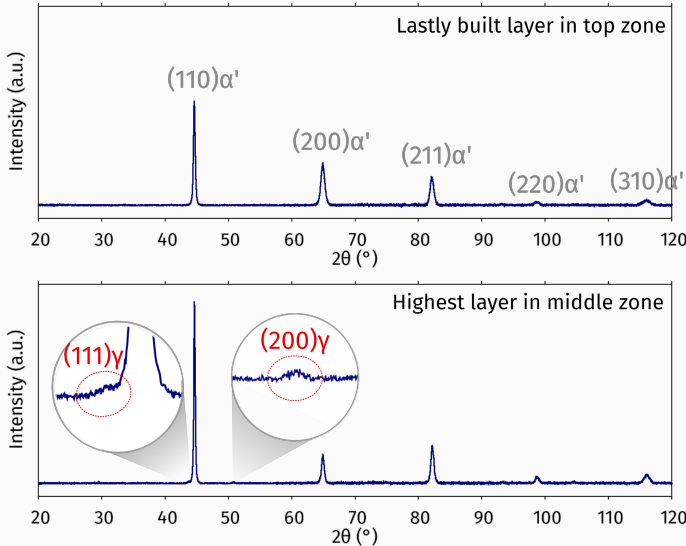


Figure: X-ray diffraction patterns.

- **Mainly martensitic microstructure.**
- **Low fraction of austenite in midled zone.**
- No detection of carbides.

Nature of the phases

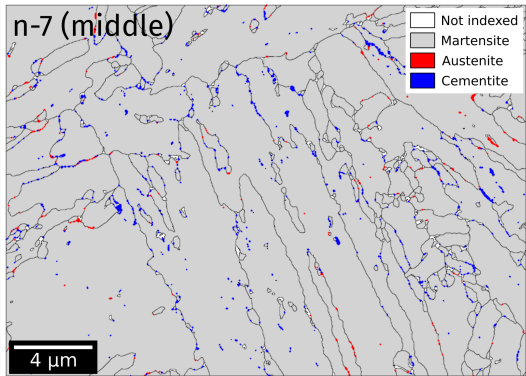


Figure: EBSD phase map in **middle zone**.

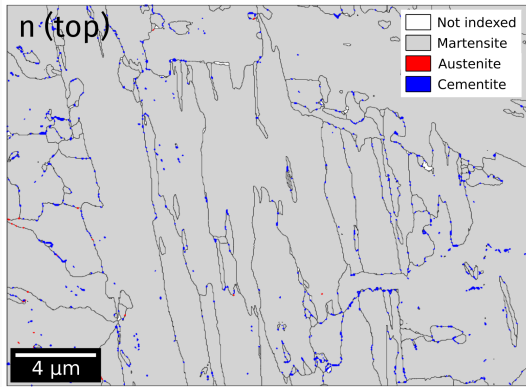


Figure: EBSD phase map in **top zone**.

Phase proportions, morphologies and localization

Table: Phase proportion from EBSD data in layers of different zones.

phase (surf%)	n-7 (middle)	n (top)
Martensite	96.73	98.91
Austenite	0.13	0.08
Cementite	0.67	0.35
Non indexed	2.47	0.66

Austenite and cementite proportions are higher in middle zone.

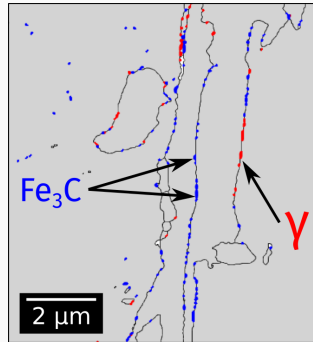
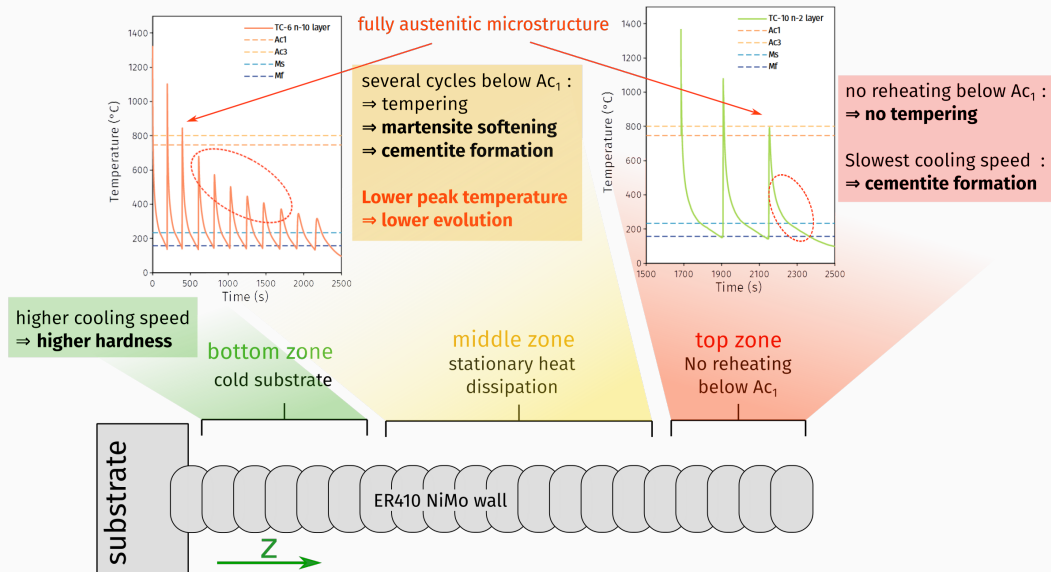


Figure: Formation of nanometric austenite and cementite in n-7 layer (middle zone).

Nanometric austenite and cementite particules are located at block boundaries.

Discussion : differences between the zones



Conclusions & perspectives

Conclusions

- Successful elaboration of ER410 NiMo thin wall by WAAM.
- 3 thermal histories \Rightarrow **3 zones** along building direction.
- Hardness oscillations delimited the different layers.
- Experimental martensitic orientation relationships **close to KS and NW** relationships.
- Higher number of sub-critical thermal cycles \Rightarrow **higher proportion of cementite.**

Perspectives

Microstructural characterization at finer scale :

- Hardness oscillations in 1 layer : *Thermal inhomogeneities, hardness contributions ...*
- Austenite : *Residual ? Reversion ?*
- Martensite : *Fresh ? Tempered ?*
- Other carbides ?

Phase field modelling

Thank you for your attention !

NISHIYAMA-WASSERMANN variants list

O.R. ^a	fcc plane ^b	bcc plane	fcc direction ^c	bcc direction	Bain Variant ^d
NW1	$(111)_{\gamma}$	$(011)_{\alpha'}$	$[10\bar{1}]_{\gamma}$	$[100]_{\alpha'}$	B_2
NW2	$(111)_{\gamma}$	$(011)_{\alpha'}$	$[\bar{1}10]_{\gamma}$	$[100]_{\alpha'}$	B_3
NW3	$(111)_{\gamma}$	$(011)_{\alpha'}$	$[0\bar{1}1]_{\gamma}$	$[100]_{\alpha'}$	B_1
NW4	$(\bar{1}11)_{\gamma}$	$(011)_{\alpha'}$	$[101]_{\gamma}$	$[100]_{\alpha'}$	B_2
NW5	$(\bar{1}11)_{\gamma}$	$(011)_{\alpha'}$	$[\bar{1}\bar{1}0]_{\gamma}$	$[100]_{\alpha'}$	B_3
NW6	$(\bar{1}11)_{\gamma}$	$(011)_{\alpha'}$	$[01\bar{1}]_{\gamma}$	$[100]_{\alpha'}$	B_1
NW7	$(1\bar{1}1)_{\gamma}$	$(011)_{\alpha'}$	$[\bar{1}01]_{\gamma}$	$[100]_{\alpha'}$	B_2
NW8	$(1\bar{1}1)_{\gamma}$	$(011)_{\alpha'}$	$[110]_{\gamma}$	$[100]_{\alpha'}$	B_3
NW9	$(1\bar{1}1)_{\gamma}$	$(011)_{\alpha'}$	$[0\bar{1}\bar{1}]_{\gamma}$	$[100]_{\alpha'}$	B_1
NW10	$(11\bar{1})_{\gamma}$	$(011)_{\alpha'}$	$[\bar{1}0\bar{1}]_{\gamma}$	$[100]_{\alpha'}$	B_2
NW11	$(11\bar{1})_{\gamma}$	$(011)_{\alpha'}$	$[1\bar{1}0]_{\gamma}$	$[100]_{\alpha'}$	B_3
NW12	$(11\bar{1})_{\gamma}$	$(011)_{\alpha'}$	$[011]_{\gamma}$	$[100]_{\alpha'}$	B_1

^a NW j ^b $P_{2j-1}(111)_{\gamma}$ ^c $\mathbf{v}_j = P_{2j-1}[10\bar{1}]_{\gamma}$ ^d $B_j = P_{2j-1}B_2P_{2j-1}^T$

Figure: List of NISHIYAMA-WASSERMANN variants and corresponding BAIN variants¹.

¹K. Koumatos, A. Muehlemann, *Acta Crystallographica Section A: Foundations and Advances* **2017**, 73, Number: 2 Publisher: International Union of Crystallography, 115–123.

Dilatometry for phase transformation temperatures

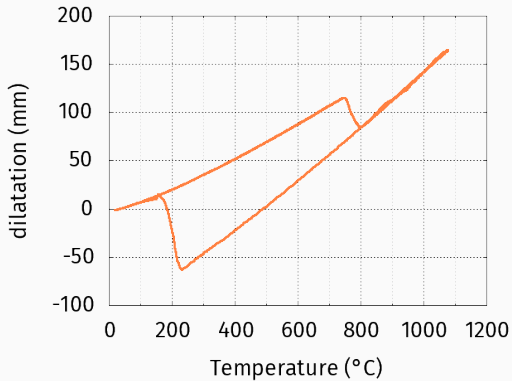


Figure: Dilatometry cycle for (n)_CT1 sample.

Table: Phase transformation temperatures measured by dilatometry (°C).

sample	Ac ₁	Ac ₃	M _s	M _f
(n)_CT1	747	800	232	156
(n)_CT2	752	812	229	152
(n-1)_CT2	733	760	250	150
Average	744	791	237	153